

Backward bifurcation underlies rich dynamics in simple disease models ^{*}

Wenjing Zhang [†] Pei Yu, ^{‡§} Lindi M. Wahl ^{¶||}

October 29, 2018

Abstract

In this paper, dynamical systems theory and bifurcation theory are applied to investigate the rich dynamical behaviours observed in three simple disease models. The 2- and 3-dimensional models we investigate have arisen in previous investigations of epidemiology, in-host disease, and autoimmunity. These closely related models display interesting dynamical behaviors including bistability, recurrence, and regular oscillations, each of which has possible clinical or public health implications. In this contribution we elucidate the key role of backward bifurcation in the parameter regimes leading to the behaviors of interest. We demonstrate that backward bifurcation facilitates the appearance of Hopf bifurcations, and the varied dynamical behaviors are then determined by the properties of the Hopf bifurcation(s), including their location and direction. A Maple program developed earlier is implemented to determine the stability of limit cycles bifurcating from the Hopf bifurcation. Numerical simulations are presented to illustrate phenomena of interest such as bistability, recurrence and oscillation. We also discuss the physical motivations for the models and the clinical implications of the resulting dynamics.

1 Keywords

Convex incidence rate, backward bifurcation, supercritical and subcritical Hopf bifurcations, recurrence, bistability, disease model

2 Mathematics Subject Classification (2000)

34C • 34D • 92B • 92D

^{*}This work was supported by the Natural Sciences and Engineering Research Council of Canada (NSERC).

[†]Wenjing Zhang, email: zhang.wenjing14@gmail.com

[‡]Pei Yu, email: pyu@uwo.ca

[§]Applied Mathematics, Western University, London, Ontario, Canada N6A 5B7

[¶]Lindi M. Wahl, email: lwahl@uwo.ca

^{||}Applied Mathematics, Western University, London, Ontario, Canada N6A 5B7

3 Introduction

In the mathematical modelling of epidemic diseases, the fate of the disease can be predicted through the uninfected and infected equilibria and their stability. The basic reproduction number, R_0 , represents the average number of new infectives introduced into an otherwise disease-free system by a single infective, and is usually chosen as the bifurcation parameter. If the model involves a forward bifurcation, the uninfected equilibrium is in general globally asymptotically stable [28], characterized by $R_0 < 1$, and infection fails to invade in this parameter regime. The threshold $R_0 = 1$ defines a bifurcation (or critical) point, and when $R_0 > 1$, a stable infected equilibrium emerges. This simple exchange of stability implies that complex dynamics will not typically occur in forward bifurcation.

In contrast, backward bifurcation describes a scenario in which a turning point of the infected equilibrium exists in a region where all state variables are positive, and $R_0 < 1$. This induces multiple infected equilibria, disrupting the global stability of the uninfected equilibrium. Multiple stable states (e.g., bistability) may likewise appear in [15, 4, 2], and Yu et al. (submitted for publication). Instead of converging globally to the uninfected equilibrium when $R_0 < 1$, the solution may approach an infected equilibrium, depending on initial conditions.

In practice, the phenomenon of backward bifurcation gives rise to new challenges in disease control, since reducing R_0 such that $R_0 < 1$ is not sufficient to eliminate the disease [22, 5]. Instead, R_0 needs to be reduced past the critical value given by the turning point [22], since the result in Yu et al. (submitted for publication) shows that the uninfected equilibrium in backward bifurcation is globally stable if R_0 is smaller than the turning point. Furthermore, an infective outbreak or catastrophe may occur if R_0 increases and crosses unity, while the upper branch of the infected equilibrium remains stable [15, 21, 47, 48]. In addition, oscillation or even recurrent phenomena may occur if uninfected and infected equilibria coexist in a parameter range, and both are unstable [47, 48]. [22] predicted oscillations arising from backward bifurcation, and [5] pointed out that the unstable infected equilibrium “commonly arises from Hopf bifurcation”, but did not demonstrate oscillations.

Several mechanisms leading to backward bifurcation have been proposed, such as partially effective vaccination programs [5, 2], educational influence on infectives’ behavior [22], the interaction among multi-group models [9, 10, 25] and multiple stages of infection [40]. In this study, we will investigate the emergence of backward bifurcation in three simple disease models which have arisen in the study of epidemiology, in-host disease and autoimmunity. In each case, we find that backward bifurcation facilitates the emergence of Hopf bifurcation(s), and Hopf bifurcation in turn underlies a range of complex and clinically relevant dynamical behaviors.

A central theme in our investigation is the role of the incidence rate in the epidemiological and in-host disease models. The incidence rate describes the speed at which an infection spreads; it denotes the rate at which susceptibles become infectives. Under the assumptions of mass action, incidence is written as the product of the infection force and the number of susceptibles. For example, if S and I denote the susceptible and infective population size respectively, a bilinear incidence rate, $f(S, I) = \beta SI$ (where β is a positive constant), is linear in each of the state variables: S and I .

The possibility of saturation effects [8, 7] has motivated the modification of the incidence rate from bilinear to nonlinear. Saturation occurs when the number of susceptible contacts per infective drops off as the proportion of infectives increases. A nonlinear incidence rate, therefore, typically increases sublinearly with respect to the growth of the infective population, and may finally reach an upper bound. The development of nonlinear incidence was first investigated in the form $\beta I^p S^q$, where β , p , and q are positive constants [32, 31, 23, 24, 13, 29]. Other forms of nonlinear incidence have also been analysed, such as $kI^p S/(1 + \alpha I^l)$ [32], and $kS \ln(1 + vP/k)$ [6].

Since the nonlinear incidence functions described above were often developed to incorporate saturation effects, these functions are typically concave at realistic parameter values. [28] used this feature to derive general results for disease models with concave incidence. They proved that standard epidemiological models with concave incidence functions will have globally asymptotically stable uninfected and infected equilibria for $R_0 < 1$ and $R_0 > 1$, respectively.

More specifically, denoting the incidence rate function as $f(S, I, N)$, where N is the population size, the classical SIRS model considered in [28] takes the form

$$\frac{dS}{dt} = \mu N - f(S, I, N) - \mu S + \alpha R, \quad \frac{dI}{dt} = f(S, I, N) - (\delta + \mu)I, \quad \frac{dR}{dt} = \delta I - \alpha R - \mu R, \quad (1)$$

where μ , δ , and α represent the birth/death rate, the recovery rate and the loss of immunity rate, respectively. When $\alpha = 0$, system (1) becomes an SIR model. Assuming that the total population size is constant, that is, $N = S + I + R$, the above system can be reduced to a 2-dimensional model:

$$\frac{dS}{dt} = (\alpha + \mu)N - f(S, I, N) - \alpha I - (\alpha + \mu)S, \quad \frac{dI}{dt} = f(S, I, N) - (\delta + \mu)I. \quad (2)$$

Moreover, it is assumed in [28] that the function $f(S, I, N)$, denoting the incidence rate, satisfies the following three conditions:

$$f(S, 0, N) = f(0, I, N) = 0, \quad (3a)$$

$$\frac{\partial f(S, I, N)}{\partial I} > 0, \quad \frac{\partial f(S, I, N)}{\partial S} > 0, \quad \forall S, I > 0 \quad (3b)$$

$$\frac{\partial^2 f(S, I, N)}{\partial I^2} \leq 0, \quad \forall S, I > 0. \quad (3c)$$

The first two conditions (3a) and (3b) are necessary to ensure that the model is biologically meaningful. The third condition (3c) implies that the incidence rate $f(S, I, N)$, is concave with respect to the number of infectives. It is also assumed that $\frac{\partial f(S, I, N)}{\partial I}$ evaluated at the uninfected equilibrium is proportional to the basic reproduction number R_0 [42], and thus should be a positive finite number [28]. Korobeinikov and Maini first considered $\dot{I} = 0$, or $f(S, I, N) - (\delta + \mu)I = 0$, and showed that forward bifurcation occurs in model (2) with a concave incidence function. They further proved that the uninfected equilibrium $Q_0 = (S_0, I_0) = (N, 0)$ and the infected equilibrium $\bar{Q} = (\bar{S}, \bar{I})$ are globally asymptotically stable, when $R_0 = \frac{1}{\delta + \mu} \frac{\partial f(S_0, I_0, N)}{\partial I} < 1$ and $R_0 > 1$, respectively.

In the sections to follow, for an incidence rate function $f(S, I)$, satisfying (3a) and (3b), we define $f(S, I)$ as concave, if it satisfies (3c); as convex, if $\frac{\partial^2 f(S, I)}{\partial I^2} > 0, \forall I > 0$; and as convex-concave, if there exist $0 < I_1 < I_2 \leq +\infty$, such that $\frac{\partial f(S, I)}{\partial I} > 0, \forall I \in (0, I_2)$, and $\frac{\partial^2 f(S, I)}{\partial I^2} > 0, \forall I \in (0, I_1)$, $\frac{\partial^2 f(S, I)}{\partial I^2} = 0$, for $I = I_1$, $\frac{\partial^2 f(S, I)}{\partial I^2} < 0, \forall I \in (I_1, I_2)$.

Several models closely related to (2) have been previously studied. For example, by adding a saturating treatment term to model (2) with a concave incidence rate, [49] showed that this model may yield backward bifurcation and Hopf bifurcation. With an even more sophisticated nonlinear incidence rate function: $kI^p S / (1 + \alpha I^l)$, where $p = l = 2$, [38] proved that a reduced 2-dimensional SIRS model could exhibit backward bifurcation, Hopf bifurcation, and even Bogdanov-Takens bifurcation and homoclinic bifurcation. Although the choice of $p = l = 2$ was not motivated by a specific physical process, this important result demonstrates that a nonlinear incidence rate can induce backward bifurcation, and further generate complex dynamics in a simple disease model.

One of the focal points of our study will be a convex incidence function which arose in a 4-dimensional HIV antioxidant therapy model [43]. In this model, the infectivity of infected cells was proposed to be an increasing function of the density of reactive oxygen species, which themselves increase as the infection progresses. In [43], meaningful parameter values were carefully chosen by data fitting to both experimental and clinical results. In this parameter regime, the model was observed to capture the phenomenon of viral blips, that is, long periods of undetectable viral load punctuated by brief episodes of high viral load. Viral blips have been observed clinically in HIV patients under highly active antiretroviral therapy [11, 14, 35, 34], and have received much attention in the research literature, both by experimentalists [17, 18, 20] and mathematicians [16, 27, 12, 37, 36]. Nonetheless, the mechanisms underlying this phenomenon are still not thoroughly understood [20, 36].

We recently re-examined the model developed in [43], with the aim of providing new insight into the mechanism of HIV viral blips [47, 48]. Focusing on the dynamics of the slow manifold of this model, we reduced the dimension of the 4-dimensional model by using quasi-steady state assumptions. After a further generalization and parameter rescaling process, a 2-dimensional in-host HIV model [47, 48] was obtained, given by

$$\frac{dX}{d\tau} = 1 - DX - \left(B + \frac{AY}{Y+C}\right)XY, \quad \frac{dY}{d\tau} = \left(B + \frac{AY}{Y+C}\right)XY - Y, \quad (4)$$

where X and Y denote the concentrations of the uninfected and infected cells respectively. The constant influx rate and the death rate of Y have been scaled to 1. The death rate of X is D . The 2-dimensional infection model above (4), reduced from the 4-dimensional HIV model [43], preserves the viral blips observed in the HIV model.

Importantly, system (4) is equivalent to the SIR model (2), except that the incidence function is convex, as we will show in section 4.2. This equivalence can be demonstrated if we set $S = e_1 x$, $I = e_2 y$, and $t = e_3 \tau$ with $e_1 = e_2 = \frac{\mu N}{\delta + \mu}$ and $e_3 = \frac{1}{\delta + \mu}$. In this case, system (2) is rescaled to

$$\frac{dx}{d\tau} = 1 - \frac{\mu}{\delta + \mu}x - \frac{1}{\mu N}f(x, y), \quad \frac{dy}{d\tau} = \frac{1}{\mu N}f(x, y) - y,$$

which takes the same form as system (4). Therefore, although system (2) arises in epidemiology and system (4) was derived as an in-host model, they are mathematically equivalent in

this sense. We will refer to both systems (2) and (4) as infection models.

In previous work [47, 48], we analyze the recurrent behavior which emerges in system (4) in some detail. Recurrence is a particular form of oscillatory behavior characterized by long periods of time close to the uninfected equilibrium, punctuated by brief episodes of high infection [45]. Thus HIV viral blips are an example of recurrent behavior, but recurrence is a more general feature of many diseases [45, 48]. We have demonstrated that the increasing and saturating infectivity function of system (4) is critical to the emergence of recurrent behaviour. This form of an infectivity function corresponds to a convex incidence rate function in the associated 2-dimensional infection model (4), and can likewise induce recurrence in this model. Convex incidence has been previously suggested to model ‘cooperation effects’ in epidemiology [28], or cooperative phenomena in reactions between enzyme and substrate, as proposed by [33].

The rest of this paper is organized as follows. In Section 2, we study two 2-dimensional infection models, both closely related to system (2). We show that system (2) with either (a) a concave incidence rate and saturating treatment term or (b) a convex incidence rate as shown in system (4), can exhibit backward bifurcation; we then identify the necessary terms in the system equations which cause this phenomenon. In Section 3, we demonstrate that in both models, backward bifurcation increases the likelihood of a Hopf bifurcation on the upper branch of the infected equilibrium. Studying system (4) in greater detail, we illustrate how the location of the Hopf bifurcations and their directions (supercritical or subcritical), determine the possible dynamical behaviors, concluding that backward bifurcation facilitates Hopf bifurcation(s), which then underly the rich behaviours observed in these models. In Section 4, we explore backward bifurcation further, presenting an autoimmune disease model which exhibits negative backward bifurcation, that is, a bifurcation for which the turning point when $R_0 < 1$ is located in a region where one or more state variables is negative. Although this bifurcation introduces two branches of the infected equilibrium, we demonstrate that, in the biologically feasible area, only forward bifurcation exists in this model. We then present a modification to this autoimmune model, motivated by the recent discovery of a new cell type, which generates a negative backward bifurcation and Hopf bifurcation, and allows recurrent behavior to emerge. A conclusion is drawn in Section 5.

4 Backward bifurcation

In this section, we study backward bifurcation in two 2-dimensional infection models. In particular, we explore the essential terms and parameter relations which are needed to generate backward bifurcation. Furthermore, we examine the convex incidence rate, and reveal its underlying role in determining the emergence of backward bifurcation.

4.1 Backward bifurcation in the infection model with concave incidence

First, we consider the SIR model with concave incidence, described by the following equations [49]:

$$\frac{dS}{dt} = \Lambda - \frac{\beta SI}{1+kI} - dS, \quad \frac{dI}{dt} = \frac{\beta SI}{1+kI} - (d + \gamma + \varepsilon)I, \quad \frac{dR}{dt} = \gamma I - dR, \quad (5)$$

where S , I and R denote the number of susceptible, infective, and recovered individuals, respectively; Λ is the constant recruitment rate of susceptibles; d , γ , and ε represent the rates of natural death, recovery, and the disease-induced mortality, respectively. Note that the function $\frac{\beta SI}{1+kI}$ is an incidence rate of the form $\frac{kI^l S}{1+\alpha I^h}$ [32], when $l = h = 1$. Here, β is the infection rate, and k measures the inhibition effect. Since the variable R is not involved in the first two equations, system (5) can be reduced to a 2-dimensional model as

$$\frac{dS}{dt} = \Lambda - \frac{\beta SI}{1+kI} - dS, \quad \frac{dI}{dt} = \frac{\beta SI}{1+kI} - (d + \gamma + \varepsilon)I. \quad (6)$$

In [49], an additional assumption regarding limited medical treatment resources is introduced to the above model, leading to a model with a saturating treatment term, given by

$$\frac{dS}{dt} = f_1(S, I) = \Lambda - \frac{\beta SI}{1+kI} - dS, \quad \frac{dI}{dt} = f_2(S, I) = \frac{\beta SI}{1+kI} - (d + \gamma + \varepsilon)I - \frac{\alpha I}{\omega + I}, \quad (7)$$

where the real, positive parameter α represents the maximal medical resources per unit time, and the real, positive parameter ω is the half-saturation constant. For simplicity, let the functions on the right-hand side of the equations in (7) be f_1 and f_2 , respectively. Then, the equilibrium solutions of system (7) are obtained by solving the following algebraic equations: $f_1(S, I) = 0$ and $f_2(S, I) = 0$, from which the disease-free equilibrium can be easily obtained as $\bar{E}_0 = (\Lambda/d, 0)$. For the infected equilibrium $\bar{E} = (\bar{S}, \bar{I})$, \bar{S} is solved from $f_1 = 0$ as $\bar{S}(I) = \frac{\Lambda(1+kI)}{(dk + \beta)I + d}$. Then, substituting $S = \bar{S}(I)$ into $f_2 = 0$ yields a quadratic equation of the form

$$\mathcal{F}(I) = \mathcal{A}I^2 + \mathcal{B}I + \mathcal{C} = 0, \quad (8)$$

which in turn gives two roots: $\bar{I}_{1,2} = \frac{-\mathcal{B} \pm \sqrt{\mathcal{B}^2 - 4\mathcal{A}\mathcal{C}}}{2\mathcal{A}}$, where, $\mathcal{A} = (d + \gamma + \varepsilon)(dk + \beta)$, $\mathcal{B} = [(dk + \beta)\omega + d](d + \gamma + \varepsilon) + (dk + \beta)\alpha - \beta\Lambda$, $\mathcal{C} = [(d + \gamma + \varepsilon)\omega + \alpha]d - \beta\Lambda\omega$ for system (7). Since all parameters take positive values, we have $\mathcal{A} > 0$. To get the two positive roots essential for backward bifurcation, it is required that $\mathcal{B} < 0$ and $\mathcal{C} > 0$. Noticing that $\beta, \Lambda, \omega > 0$, we can see that the infection force, β , the constant influx of the susceptibles, Λ , and the effect of medical treatment $\frac{\alpha I}{\omega + I}$ are indispensable terms for backward bifurcation. The number of positive infected equilibrium solutions changes from two to one when the value of \mathcal{C} passes from negative to positive, which gives a critical point at $\mathcal{C} = 0$, that is, $[(d + \gamma + \varepsilon)\omega + \alpha]d = \beta\Lambda\omega$, which is equivalent to $R_0 = \frac{\beta\Lambda}{(d + \gamma + \varepsilon + \alpha/\omega)d} = 1$.

On the other hand, we may infer the emergence of backward bifurcation without solving the equilibrium conditions. If we do not consider the medical treatment term $\frac{\alpha I}{\omega + I}$ and remove it from system (7), that leads to system (6), which is a typical example of an SIR model studied by (2). By setting the incidence function as $f_3(S, I) = \frac{\beta SI}{1+kI}$, we have $f_3(0, I) = f_3(S, 0) = 0$;

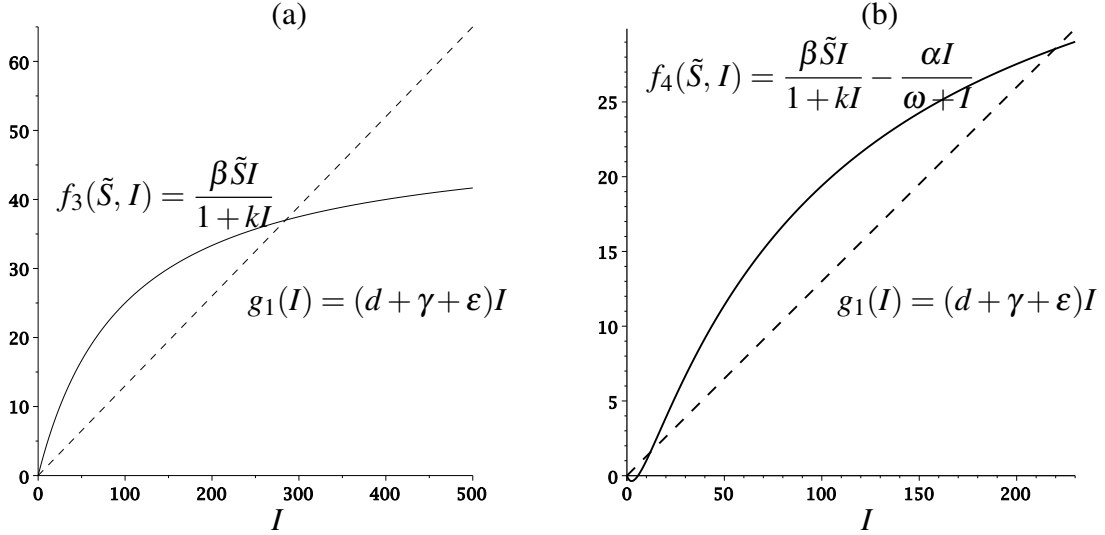


Figure 1: Graphs of the incidence function f_3 in system (5), (6) and function f_4 in system (7) with respect to I , for which $\tilde{S} = 50$ has been used. The parameter values are chosen as $\beta = 0.01$, $k = 0.01$, $\alpha = 6$, $\omega = 7$, $d = 0.1$, $\gamma = 0.01$, $\varepsilon = 0.02$, according to [49]. The solid lines denote f_3 in (a) and f_4 in (b), while the dashed ray lines in both graphs represent $g_1(I) = (d + \gamma + \varepsilon)I$. (a) the incidence function $f_3(S, I) = \frac{\beta SI}{1+kI}$, showing one intersection point with g_1 ; and (b) the function $f_4(S, I) = \frac{\beta SI}{1+kI} - \frac{\alpha I}{\omega+I}$, showing two intersection points with g_1 .

$\frac{\partial f_3(S, I)}{\partial S} = \frac{\beta I}{1+kI} > 0$ and $\frac{\partial f_3(S, I)}{\partial I} = \frac{\beta S}{(1+kI)^2} > 0$ for all $S, I > 0$; and $\frac{\partial^2 f_3(S, I)}{\partial I^2} = -2\beta kS(1+kI)^{-3} < 0$ for all $S, I > 0$. Therefore, the incidence function $f_3(S, I)$, satisfies the conditions given in (3). In particular, the function is concave, and can only have one intersection point with the line $(d + \gamma + \varepsilon)I$ in the I - S plane, as shown in Figure 1(a). Thus, the uniqueness of the positive infected equilibrium implies that backward bifurcation cannot occur in this case. Moreover, according to the result in [28], the uninfected and infected equilibria are globally asymptotically stable for $R_0 = \frac{\beta\Lambda}{d(d+\gamma+\varepsilon)} < 1$ and $R_0 > 1$, respectively. No complex dynamical behavior happens in system (6).

In contrast, when we introduce the loss of the infectives due to medical treatment, the dynamics of system (7) differ greatly from system (6). In particular, backward bifurcation emerges and complex dynamical behaviors may occur. To clarify this effect, we denote the function induced by $\dot{I} = 0$ from (7) as $f_4(S, I) = \frac{\beta SI}{1+kI} - \frac{\alpha I}{\omega+I}$. Note that $f_4(S, I)$ is not an incidence rate. But, if we fix $S = \tilde{S} > 0$, there exist $0 < I_1 < I_2 < +\infty$, such that $\frac{\partial f_4(\tilde{S}, I)}{\partial I} = \frac{1}{(1+kI)^2(\omega+I)^2} [\beta\tilde{S}(\omega+I)^2 - \alpha\omega(1+kI)^2] > 0, \forall I \in (0, I_2)$; and $\frac{\partial^2 f_4(\tilde{S}, I)}{\partial I^2} = -2k\beta\tilde{S}(1+kI)^{-3} + 2\alpha\omega(\omega+I)^{-3} > 0, \forall I \in (0, I_1)$, $\frac{\partial^2 f_4(\tilde{S}, I)}{\partial I^2} = 0$, for $I = I_1$, $\frac{\partial^2 f_4(\tilde{S}, I)}{\partial I^2} < 0, \forall I \in (I_1, I_2)$. Thus, $f_4(\tilde{S}, I)$ actually has a convex-concave ‘S’ shape, and may have two positive intersection points with the ray line, $g_1(I) = (d + \gamma + \varepsilon)I$, in the first quadrant; see Figure 1(b). These intersections contribute the two positive equilibrium solutions that are a necessary feature of backward bifurcation.

In summary we may conclude that the necessary terms which should be contained in system (7) in order to have backward bifurcation are the constant influx Λ , the infection force β , and the saturating medical treatment $\frac{\alpha I}{\omega + I}$.

4.2 Backward bifurcation in the infection model with convex incidence

Now we consider the 2-dimensional infection model (4) which exhibits viral blips, studied in [47, 48]. The motivation for this model was a series of clinical discoveries indicating that viral infection can increase the density of a harmful chemical substance [19, 30, 39, 26], thereby amplifying an associated biochemical reaction [41], and thus accelerating the infection rate [19]. This cooperative phenomenon in viral infection is expressed by an increasing, saturating infectivity function: $(B + \frac{AY}{Y+C})$. According to the principle of mass action, the incidence function is then denoted as $(B + \frac{AY}{Y+C})XY$, which is a convex function with respect to the infectives' density Y .

To analyze the occurrence of possible backward bifurcation, we first examine the two equilibrium solutions from the following equations:

$$f_5(X, Y) = 1 - DX - (B + \frac{AY}{Y+C})XY = 0, \quad f_6(X, Y) = (B + \frac{AY}{Y+C})XY - Y = 0, \quad (9)$$

where all parameters A, B, C and D are positive constants. It is easy to find the uninfected equilibrium $\bar{E}_0 = (\bar{X}_0, \bar{Y}_0) = (\frac{1}{D}, 0)$, whose characteristic polynomial has two roots: $\lambda_1 = -D < 0$, and $\lambda_2 = \frac{B}{D} - 1$, which gives $R_0 = \frac{B}{D}$. Consequently, \bar{E}_0 is stable (unstable) for $R_0 < 1$ (> 1). To find the infected equilibrium solution, setting $f_6(X, Y) = 0$ yields $\bar{X}_1(Y) = \frac{Y+C}{(A+B)Y+BC}$, which is then substituted into $f_5(X, Y) = 0$ to give the following quadratic equation:

$$\mathcal{F}_5(Y) = (A+B)Y^2 + (BC+D-A-B)Y + C(D-B) = 0. \quad (10)$$

In order to have two real, positive roots, two conditions must be satisfied, that is, $BC+D-A-B < 0$ and $D-B > 0$, or in compact form, $0 < D-B < A-BC$. The condition $D-B > 0$ is equivalent to $0 < R_0 = \frac{B}{D} < 1$, which is a necessary condition for backward bifurcation. Moreover, the positive influx constant, having been scaled to 1, is a necessary term for the positive equilibrium of Y . Therefore, the positive influx rate term and the increasing and saturating infectivity function are necessary for backward bifurcation.

In the rest of the subsection, we further examine the incidence function,

$$f_7(X, Y) = (B + \frac{AY}{Y+C})XY, \quad (11)$$

without solving the equilibrium solutions. The incidence function f_7 obviously satisfies the condition (3a), as well as the condition (3b) since $\frac{\partial}{\partial X} f_7(X, Y) = [B + AY(Y+C)^{-1}]Y > 0$ and $\frac{\partial}{\partial Y} f_7(X, Y) = ACXY(Y+C)^{-2} + [B + AY(Y+C)^{-1}]X > 0$ for all $X, Y > 0$. However, the second partial derivative of $f_7(X, Y)$ with respect to Y , $\frac{\partial^2}{\partial Y^2} f_7(X, Y) = 2AC^2X(X+C)^{-3} > 0$ for all $X, Y > 0$, showing that $f_7(X, Y)$ is a convex function with respect to the variable Y . Consequently, $f_7(X, Y)$ can only have one intersection with $g_2(Y) = Y$, implying that

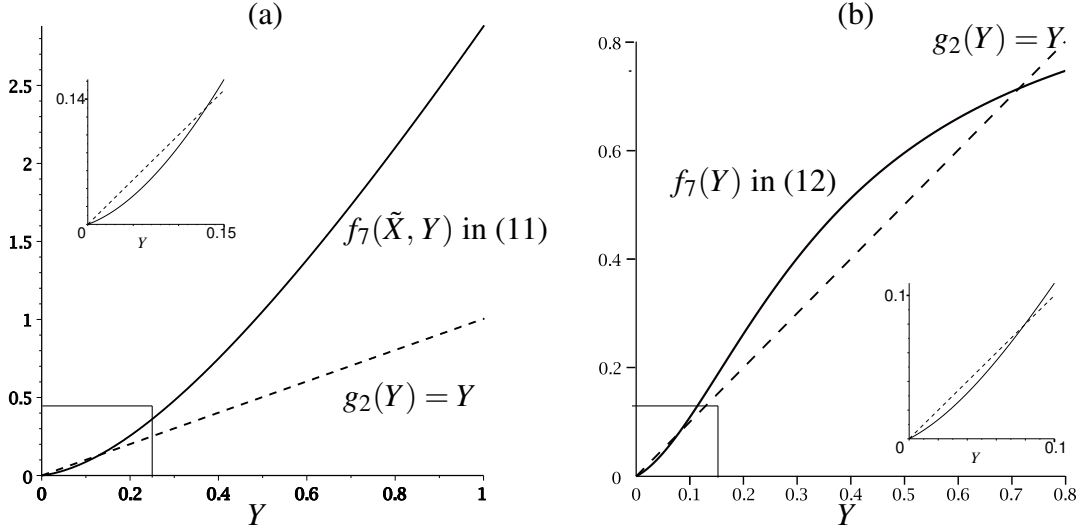


Figure 2: Graphs of the incidence functions $f_7(\tilde{X}, Y)$ and $f_7(Y)$ for the parameter values $A = 0.364$, $B = 0.03$, $C = 0.823$, and $D = 0.057$. The incidence functions are denoted by the solid lines, while the ray lines, determined by $g_2(Y) = Y$, are denoted by dotted lines: (a) the incidence function $f_7(\tilde{X}, Y)$, showing one intersection point with g_2 with an inset, with a fixed value $\tilde{X} = 12.54$; and (b) the incidence function $f_7(Y)$, showing two intersection points with an inset.

only one equilibrium solution would exist if we only consider the second equation in (9), as shown Figure 2 (a). However, when considering both conditions given in (9) for equilibrium solutions, we will have two intersection points between f_7 and g_2 . According to the first equation in (9), that is $f_5(X, Y) = 0$, we can use Y to express X in the equilibrium state as $\tilde{X}(Y) = (Y + C)[(A + B)Y^2 + (BC + D)Y + DC]^{-1}$. Substituting $\tilde{X}(Y)$ into $f_7(X, Y)$ in (11), we obtain

$$f_7(Y) = Y[(A + B)Y + BC][(A + B)Y^2 + (BC + D)Y + CD]^{-1}, \quad (12)$$

and $\frac{\partial}{\partial Y} f_7(Y) = D[(A + B)Y^2 + 2(A + B)CY + BC^2][(A + B)Y^2 + (BC + D)Y + CD]^{-2} > 0$ for all $X, Y > 0$. However, the sign of $\frac{\partial^2}{\partial Y^2} f_7(Y) = -2D[(A + B)^2Y^3 + 3C(A + B)^2Y^2 + 3(A + B)BC^2Y + (B^2C - AD)C^2][(A + B)Y^2 + (BC + D)Y + CD]^{-3}$, could alter at the inflection point from positive to negative as Y increases. Therefore, with appropriate parameter values, $f_7(Y)$ can have a convex-concave ‘S’ shape, yielding two intersection points with the ray line, $g_2(y)$, in the first quadrant of the X - Y plane, as shown in Figure 2 (b). The above discussion, as illustrated in Figure 2, implies that system (4) can have two positive equilibrium solutions when $R_0 < 1$, and thus backward bifurcation may occur.

Remark 1 *Summarizing the discussions and results given in this section indicates that a disease model with a convex-concave incidence function may lead to backward bifurcation, which in turn implies: (a) the system has at least two equilibrium solutions, and the two equilibrium solutions intersect at a transcritical bifurcation point; and (b) at least one of the equilibrium solutions is determined by a nonlinear equation.*

5 Hopf bifurcation

In the previous section, we studied backward bifurcation and established the necessary conditions for the occurrence of backward bifurcation in two models. In this section, we turn to Hopf bifurcation, since it typically underlies the change of stability in the upper branch of the infected equilibrium, the key condition in determining whether a model can exhibit oscillation or even recurrence. Again, we will present detailed studies for the two models.

5.1 Hopf bifurcation in the infection model with concave incidence

In this subsection, we study two cases of an infection model with concave incidence: system (6) and (7). First, we discuss the equilibrium solutions and their stability by using the Jacobian matrix, denoted by J , and examining the corresponding characteristic polynomial,

$$P|_J(L) = L^2 + \text{Tr}(J)L + \text{Det}(J). \quad (13)$$

Bifurcation analysis is conducted by choosing Λ as the bifurcation parameter.

First, we consider the case without saturating medical treatment, system (6). This system satisfies the three conditions in (3), and consequently, its uninfected equilibrium $\bar{E}_0 = (\frac{\Lambda}{d}, 0)$ is globally asymptotically stable if $R_0 = \frac{\beta\Lambda}{(d+\gamma+\varepsilon)d} \leq 1$, while the infected equilibrium $\bar{E}_1 = (\frac{k\Lambda+d+\gamma+\varepsilon}{dk+\beta}, \frac{\beta\Lambda-(d+\gamma+\varepsilon)d}{(dk+\beta)(d+\gamma+\varepsilon)})$ emerges and is globally asymptotically stable if $R_0 > 1$. Therefore, for this case the system has only one transcritical bifurcation point at $R_0 = 1$ and no complex dynamics can occur.

Next, with the saturating treatment term, system (7) violates the conditions established for model (3), but leads to the possibility of complex dynamical behaviors. In fact, evaluating the Jacobian matrix $J_1 = J|_{(7)}(\bar{E}_0)$ at the uninfected equilibrium, $\bar{E}_0 = (\frac{\Lambda}{d}, 0)$, yields the characteristic polynomial in the form of (13), denoted by $P|_{J_1}(L)$, with $\text{Tr}(J_1) = \left(-\frac{\beta\Lambda}{d} + \varepsilon + \frac{\alpha}{\omega} + 2d\right)$, and $\text{Det}(J_1) = \left(-\beta\Lambda + d^2 + d\varepsilon + \frac{\alpha d}{\omega}\right) = \text{Tr}(J_1)d - d^2$. This indicates that $\text{Det}(J_1) < 0$ when $\text{Tr}(J_1) = 0$, and thus Hopf bifurcation cannot occur from \bar{E}_0 . On the other hand, a static bifurcation can occur when $\text{Det}(J_1) = 0$, that is, $\Lambda_S = \frac{1}{\beta}(d^2 + d\varepsilon + \frac{\alpha d}{\omega})$, where the subscript ‘S’ refers to *static bifurcation*. Therefore, \bar{E}_0 is stable (unstable) for $\Lambda < \Lambda_S$ ($> \Lambda_S$), or $R_0 < 1$ (> 1), with $R_0 = \beta\Lambda d^{-1}(d + \gamma + \varepsilon + \frac{\alpha}{\omega})^{-1}$ [49].

We will show that complex dynamical behaviors can emerge in system (7) from the infected equilibrium $\bar{E}_1 = (\bar{S}, \bar{I})$, where \bar{I} is determined from the equation $\mathcal{F}(I) = 0$ in (8). In the Λ - I plane, the bifurcation diagram as shown in Figure 3 (1)-(4), indicates a turning point on the curve with appropriate parameter values, determined by both the quadratic equation (8) and the relation $\frac{d\Lambda}{dI} = -\frac{\partial \mathcal{F}}{\partial I} / \frac{\partial \mathcal{F}}{\partial \Lambda} = 0$, which is equivalent to $\frac{\partial \mathcal{F}}{\partial I} = 0$. Solving $\frac{\partial \mathcal{F}}{\partial I} = 0$ yields the turning point of I , denoted by I_T (‘T’ means *turning*), taking the form

$$I_T = \frac{1}{2} \left[\frac{\beta\Lambda_T}{(dk+\beta)(d+\varepsilon)} - \omega - \frac{d}{dk+\beta} - \frac{\alpha}{d+\varepsilon} \right],$$

where Λ_T is obtained from $\mathcal{F}(I_T) = 0$, see (8). Thus, when $I_T > 0$ (< 0), the turning point of the quadratic curve appears above (below) the I -axis, meaning that backward bifurcation occurs for $I > 0$ (< 0). Evaluating the Jacobian matrix at the infected equilibrium \bar{E}_1 , and further

denoting it as $J_2 = J|_{(7)}(\bar{E}_1)$, we obtain the characteristic polynomial in the form of (13), with $\text{Tr}(J_2) = a_{11}/[(\omega + I)^2(kI + 1)(dkI + \beta I + d)]$ and $\text{Det}(J_2) = a_{21}/[(\omega + I)^2(kI + 1)(dkI + \beta I + d)]$, where $a_{11} = a_{1a} - a_{1b}$ and $a_{21} = a_{2a} - a_{2b}$, with $a_{1b} = \beta\Lambda(\omega + I)^2$ and $a_{2b} = da_{1b}$, and a_{1a} and a_{2a} only contain positive terms (their expressions are omitted here for brevity). Therefore, we can rewrite $\text{Det}(J_2) = \frac{a_{21}}{d}/[(\omega + I)^2(kI + 1)(dkI + \beta I + d)]$. Determining whether a Hopf bifurcation can occur from \bar{E} is equivalent to finding whether $\text{Det}(J_2)$ remains positive when $\text{Tr}(J_2) = 0$. Ignoring the positive factors in the following subtraction yields

$$h_1(I) = \frac{\text{Tr}(J_2) - \text{Det}(J_2)/d}{(\omega + I)^2(kI + 1)(dkI + \beta I + d)} = a_{11} - \frac{1}{d}a_{21} = a_{1a} - \frac{1}{d}a_{2a},$$

where $h_1(I) = \frac{1}{d}(dkI + \beta I + d)[(kI + 1)d^2(\omega + I)^2 - \beta\epsilon I(\omega + I)^2 - \alpha\beta\omega I]$. Thus, when $a_{1a} = 0$, $\frac{1}{d}a_{2a}$ and $h_1(I)$ have opposite signs, implying that when $\text{Tr}(J_2) = 0$, $\text{Det}(J_2)$ could be positive only if $h_1(I)$ is negative. Therefore, the necessary condition for system (7) to have a Hopf bifurcation from the infected equilibrium \bar{E}_1 is that $h_1(I)$ is negative.

In the remaining part of this subsection, we demonstrate various dynamics which may happen in system (7) with different parameter values of k , as shown in Table 1. Taking other parameter values as $\alpha = 6$, $\omega = 7$, $\epsilon = 0.02$, $\gamma = 0.01$, $\beta = 0.01$, and $d = 0.1$, and solving the two equations $\text{Tr}(J_2) = 0$ and $\mathcal{F}(I) = 0$ in (8) gives the Hopf bifurcation point candidates, (Λ_H, I_H) , for which $h_1(I_H) < 0$. Since the formula for the transcritical bifurcation point Λ_S has no relation with k , $(\Lambda_S, I_S) = (9.87, 0)$ is a fixed value pair in Table 1. Bifurcation diagrams and associated numerical simulations are shown in Figure 3 corresponding to the five cases given in Table 1. The blue lines and red curves represent the uninfected equilibrium \bar{E}_0 and infected equilibrium \bar{E}_1 , respectively. The stable and unstable equilibrium solutions are shown by solid and dashed lines/curves, respectively. Backward bifurcation occurs in Cases 1, 2, and 3 (see Table 1), which are illustrated by the corresponding bifurcation diagrams in Figures 3(1), (2), and (3), respectively. For Cases 1 and 2, only one Hopf bifurcation occurs on the upper branch of the infected equilibrium \bar{E}_1 , and this bifurcation point exists at the critical point $\Lambda_H < \Lambda_S$ for Case 1 and $\Lambda_H > \Lambda_S$, for Case 2. For Case 1 with $\Lambda = 9.78$, the simulated time history converges to \bar{E}_0 with initial condition IC = [93.6, 0.44], shown in Figure 3(1a), but converges to \bar{E}_1 with initial condition IC = [46.8, 10], shown in Figure 3(1b). This clearly indicates the bistable behavior when $\Lambda_H < \Lambda_S$, and an overlapping stable region for both \bar{E}_0 and \bar{E}_1 exists (see Figure 3(1)). The recurrent behavior for Case 2 is simulated at $\Lambda = 9.87$ with IC = [50, 5], shown in Figure 3(2a). For Case 2, $\Lambda_H > \Lambda_S$, and an overlapping unstable parameter region for both \bar{E}_0 and \bar{E}_1 occurs between Λ_S and Λ_H (see Figure 3(2)). For Case 3, two Hopf bifurcations occur on the left side of Λ_S , and a stable part in the upper branch of \bar{E}_1 exists when Λ passes through the critical value $\Lambda = \Lambda_S$. In this case, although backward bifurcation still exists and the turning point is also located above the Λ -axis, giving two branches of biologically feasible \bar{E}_1 , only regular oscillating behavior is observed. The simulated time history is conducted at $\Lambda = 10$, with initial condition IC = [50, 2], shown in Figure 3(3a). For Case 4, only forward bifurcation occurs in the biologically feasible region, and the turning point for backward bifurcation moves down to the fourth quadrant, that is, negative backward bifurcation occurs in this case. The whole upper branch of \bar{E}_1 in the first quadrant is stable, therefore, no oscillations (or recurrence) can happen. Finally, further increases to the value of k change the shape of the red curves, as shown in Figure 3(5), which again indicates that no biologically meaningful backward bifurcation or oscillations can occur. Note that in Figure 3(5)

Table 1: Dynamics of system (7) for different values of k , with $\alpha = 6$, $\omega = 7$, $\varepsilon = 0.02$, $\gamma = 0.01$, $\beta = 0.01$, $d = 0.1$, and a fixed transcritical bifurcation point $(\Lambda_S, I_S) = (9.87, 0)$.

Case	k	(Λ_T, I_T)	$h_1(I) < 0$	(Λ_H, I_H)	Dynamics	Notes
1	0.001	(9.48, 4.57)	$I \in [1.72, \infty]$	(9.73, 10.28)	Bistability	$\Lambda_H < \Lambda_S$
2	0.01	(9.71, 2.82)	$I \in [1.76, \infty]$	(9.96, 8.00)	Recurrence	$\Lambda_H > \Lambda_S$
3	0.02	(9.85, 0.84)	$I \in [1.82, \infty]$	(9.88, 2.09), (10.14, 5.62)	Oscillation	Two Hopf critical points
4	0.027	(9.86, -0.65)	$I \in [1.85, 30.65]$	No Hopf	No oscillation	Negative backward bifurcation
5	0.05	No Turning	$I \in [2.01, 15.03]$	(6.18, -22.15)	No oscillation	No backward bifurcation

a Hopf bifurcation point exists on the lower branch of the equilibrium solution, which is biologically unfeasible since it is entirely below the horizontal axis. In conclusion, interesting dynamical behaviors can emerge in system (7) if backward bifurcation occurs.

5.2 Hopf bifurcation in the infection model with convex incidence

In this subsection, we return to system (4), that is, the 2-dimensional HIV model with convex incidence derived in [47, 48], and analyze the various dynamical phenomena which system (4) could possibly exhibit. To achieve this, we set B as the bifurcation parameter, and A as a control parameter; the bifurcation analysis will be carried out for various values of A . Also, simulated time histories are provided to illustrate the dynamical behavior predicted in the analysis.

We first consider the uninfected equilibrium $\bar{E}_0 = (\frac{1}{D}, 0)$, which has two eigenvalues. One of them, given by $\lambda_1|_{\bar{E}_0} = -D$, is always negative. The other one is $\lambda_2|_{\bar{E}_0} = \frac{B}{D} - 1$. Thus, depending upon the relation between B and D , $\lambda_2|_{\bar{E}_0} = 0$ gives a static bifurcation at $B_S = D$ (or $R_0 = \frac{B}{D} = 1$), which is further proved to be a transcritical bifurcation. Here the ‘S’ in subscript stands for *static bifurcation*. Therefore, \bar{E}_0 is stable when $B < D$ (or $R_0 < 1$), loses its stability and becomes unstable when B increases to pass through $B_S = D$, that is $B > D$ (or $R_0 > 1$), and no other bifurcations can happen.

Next, we examine the infected equilibrium $\bar{E}_1 = (\bar{X}, \bar{Y})$. Since $\bar{X}(Y) = \frac{Y+C}{(A+B)Y+BC}$, \bar{Y} is determined by the quadratic equation (10), which gives the turning point (B_T, Y_T) as

$$B_T = \frac{-A + D + 2\sqrt{ACD}}{C + 1}, \quad Y_T = \frac{A + B - BC - D}{A + B},$$

where ‘T’ in the subscript stands for *turning bifurcation*. We perform a further bifurcation

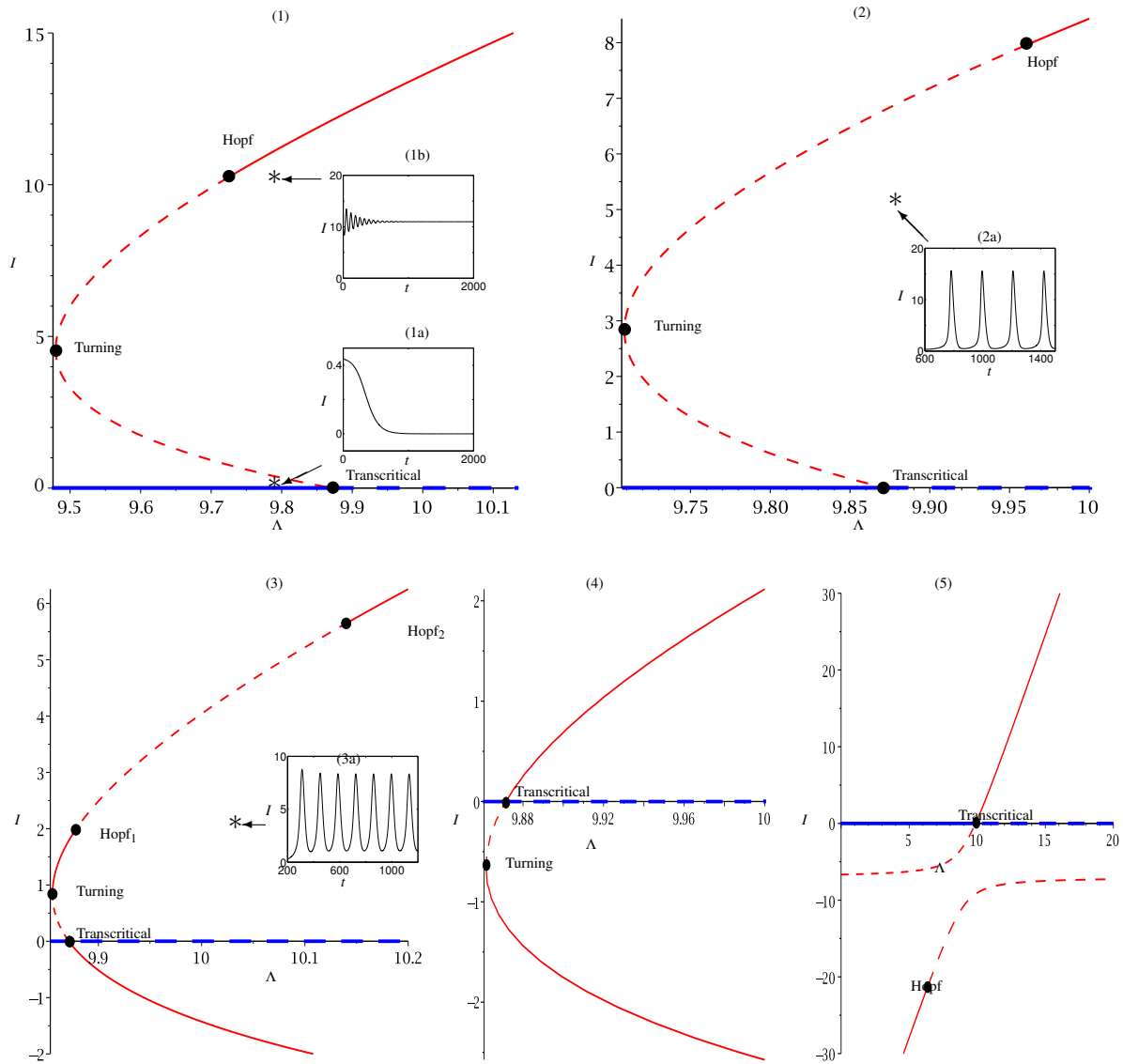


Figure 3: Bifurcation diagrams and simulations associated with the five cases given in Table 1, demonstrating various dynamical behaviors.

analysis on its corresponding characteristic polynomial (13), which takes the form

$$P|_{\bar{E}_1}(\lambda, Y) = \lambda^2 + \frac{a_{1a}}{[(A+B)Y+BC](Y+C)}\lambda + \frac{a_{2a}}{[(A+B)Y+BC](Y+C)}, \quad \text{where} \\ a_{1a} = (A+B)^2Y^3 + (2BC+D)(A+B)Y^2 + (B^2C^2+ACD+2BCD-AC)Y + BC^2D, \\ a_{2a} = (A+B)^2Y^3 + 2(A+B)BCY^2 + (B^2C-AD)CY. \quad (14)$$

Therefore, the sign of the subtraction between the trace and determinant is determined by $h_2(Y) = a_{1a} - a_{2a} = D(A+B)Y^2 + [2CD(A+B) - AC]Y + BC^2D$. Here the equilibrium solution of Y and other parameters satisfy the quadratic equation (10), which leads to an explicit expression, given by $\bar{B} = -\frac{AY^2+(D-A)Y+CD}{Y^2+(C-1)Y-C}$. Substituting $B = \bar{B}$ into $h_2(Y)$, we obtain

$$h_2(Y)|_{B=\bar{B}} = a_{1a} - a_{2a} = \frac{[AC(D-1) - D^2]Y^2 - [AC(D-1) + 2CD^2]Y - C^2D^2}{Y-1}.$$

Hopf bifurcation may occur when the trace is zero, while the determinant is still positive. This implies $h_2(Y) < 0$, which is possible with appropriately chosen parameter values. Hence, by solving $a_{1a} = 0$ in (14) together with the quadratic equation (10), we get two pairs of points denoted by (B_{h1}, Y_{h1}) and (B_{h2}, Y_{h2}) , which are candidates for Hopf bifurcation. Then validating the above two points by substituting them back into the characteristic polynomial (14), respectively, we denote the Hopf bifurcation point as (B_H, Y_H) if this validation confirms their existence. According to (Yu et al., submitted for publication), Hopf bifurcation can happen only from the upper branch of the infected equilibrium \bar{E}_1 .

The various dynamical behaviors which may appear in system (4) have been classified in Table 2 for different values of the parameter A , with fixed values of $C = 0.823$ and $D = 0.057$. Thus, the transcritical bifurcation point is fixed for all cases: $B_S = D = 0.057$ and $Y_S = 0$. The two solutions B_{h1} and B_{h2} are solved from the two equations (14) $P|_{\bar{E}_1}(\lambda, Y) = 0$ and (10) $\mathcal{F}_5(Y) = 0$, respectively. They become a Hopf bifurcation point only if their corresponding Y values (Y_{h1} and Y_{h2} , respectively) are in the range such that $h_2(Y) < 0$. Otherwise, system (4) has a pair of real eigenvalues with opposite signs at (B_{h1}, Y_{h1}) or (B_{h2}, Y_{h2}) , which is denoted by the superscript ‘*’ (which is actually a saddle point) in Table 2, while the Hopf bifurcation point is denoted by the superscript ‘H’ in Table 2.

Next, we further examine the direction of the Hopf bifurcation, that is, check whether it is a supercritical or subcritical Hopf bifurcation. Since the Jacobian matrix of the system evaluated at the Hopf bifurcation point has a pair of purely imaginary eigenvalues, the linearized system (4) does not determine the nonlinear behavior of the system. Therefore, we take advantage of normal form theory to study the existence of the limit cycles bifurcating from the Hopf bifurcation point as well as their stability. As mentioned earlier, Hopf bifurcation can only occur from the upper branch of the infected equilibrium \bar{E}_1 , therefore we first transform the fixed point \bar{E}_1 to the origin by a shifting transformation, and, in addition, make the parameter transformation $B = B_H + \mu$; the Hopf bifurcation point is thus defined as $\mu = \mu_H = 0$. Then the normal form of system (4) near the critical point, $\mu = \mu_H = 0$, takes the form up to third-order approximation:

$$\dot{r} = d\mu r + ar^3 + \mathcal{O}(r^5), \quad \dot{\theta} = \omega_c + c\mu + br^2 + \mathcal{O}(r^4), \quad (15)$$

Table 2: Parameter values taken to illustrate various dynamics of system (4). The fixed transcritical bifurcation point: $(B_S, Y_S) = (0.057, 0)$

Case	A	(B_T, Y_T)	$h_2(Y) < 0, Y \in$	(B_{h1}, Y_{h1})
1	0.80	$(-0.1950, 0.5850)$	$(0.0036, 0.9830)$	$(0.0355, 0.8725)^H$
2	0.71	$(-0.1580, 0.5660)$	$(0.0040, 0.9800)$	$(0.0539, 0.0038)^*$
3	0.60	$(-0.1140, 0.5380)$	$(0.0048, 0.9769)$	$(0.0540, 0.0045)^*$
4	0.07	$(0.0557, 0.0909)$	$(0.0476, 0.8030)$	$(0.0560, 0.0470)^*$
5	0.06	$(0.056558, 0.05581)$	$(0.0574, 0.7700)$	$(0.056559, 0.0574)^H$
6	0.05	$(0.05697, 0.01442)$	$(0.0724, 0.7232)$	$(0.0574, 0.0741)^H$
7	0.04	$(0.0569, -0.0358)$	$(0.0986, 0.6507)$	$(0.0592, 0.1071)^H$
8	0.03	$(0.0559, -0.0994)$	$(0.1611, 0.5149)$	—

Case	A	(B_{h2}, Y_{h2})	Dynamics	Notes
1	0.80	$(0.054, 0.0034)^*$	Unstable limit cycle, Bistable	$B_{h1} < B_S$
2	0.71	$(0.0574, 0.8650)^H$	Recurrence	$B_{h2} > B_S$
3	0.60	$(0.0819, 0.8530)^H$	Recurrence	$B_{h2} > B_S$
4	0.07	$(0.1015, 0.5612)^H$	Recurrence	$B_{h2} > B_S$
5	0.06	$(0.0961, 0.5225)^H$	Recurrence	$B_{h1} < B_S < B_{h2}$
6	0.05	$(0.0894, 0.4701)^H$	Recurrence	$B_{h1} < B_S < B_{h2}$
7	0.04	$(0.0806, 0.3897)^H$	Oscillation	$B_{h1} < B_S < B_{h2},$ $Y_T < 0$
8	0.03	—	\bar{E}_1 stable	$Y_T < 0$

Table 3: Classification of Hopf bifurcations based on the normal form (15).

Class	Stability of $\bar{r} = 0$		Stability of $\bar{r}^2 = -\frac{d\mu}{a}$		Hopf bifurcation
	$\mu < 0$	$\mu > 0$	$\mu < 0$	$\mu > 0$	
(a): $d > 0, a > 0$	stable	unstable	unstable	–	subcritical
(b): $d > 0, a < 0$	stable	unstable	–	stable	supercritical
(c): $d < 0, a > 0$	unstable	stable	–	unstable	subcritical
(d): $d < 0, a < 0$	unstable	stable	stable	–	supercritical

Table 4: Classification of Hopf bifurcations appearing in Table 2.

Case	A	Hopf bifurcation point (B_H, Y_H)	d	a	Stability of limit cycles	Table 3 class
1	0.8	(0.0355, 0.8725)	–1.0722	0.2114×10^{-2}	Unstable	(c)
2	0.71	(0.0574, 0.8650)	–1.0726	0.1424×10^{-2}	Unstable	(c)
3	0.6	(0.0819, 0.8530)	–1.0733	0.6755×10^{-3}	Unstable	(c)
4	0.07	(0.1015, 0.5612)	–1.0307	-0.8791×10^{-3}	stable	(d)
5	0.06	(0.056559, 0.0574)	884.27	–0.1019	Stable	(b)
		(0.0961, 0.5225)	–1.0079	-0.8613×10^{-3}	Stable	(d)
6	0.05	(0.0574, 0.0741)	18.232	-0.3145×10^{-2}	Stable	(b)
		(0.0894, 0.4701)	–0.9629	-0.8457×10^{-3}	Stable	(d)
7	0.04	(0.0592, 0.1071)	4.7242	-0.1577×10^{-2}	Stable	(b)
		(0.0805, 0.3897)	–0.8437	-0.8438×10^{-3}	Stable	(d)

where r and θ represent the amplitude and phase of the motion, respectively. The first equation of (15) can be used for bifurcation and stability analysis, while the second equation of (15) can be used to determine the frequency of the bifurcating periodic motions. The positive ω_c in the second equation of (15) is the imaginary part of the eigenvalues at the Hopf bifurcation point. The parameters d and c can be easily obtained from a linear analysis, while a and b must be derived using a nonlinear analysis, with the Maple program available in, say, [46].

Note that the infected equilibrium \bar{E}_1 is represented by the fixed point $\bar{r} = 0$ of system (15), while the nonzero fixed point $\bar{r} > 0$ (satisfying $\bar{r}^2 = -\frac{d\mu}{a}$) is an approximate solution for a limit cycle or periodic orbit. The periodic orbit is asymptotically stable (unstable) if $a < 0$ ($a > 0$), and the corresponding Hopf bifurcation is called supercritical (subcritical). According to the Poincare-Andronov Hopf Bifurcation theorem [44], for μ sufficiently small, there are four possibilities for the existence of periodic orbits and their stability, which are classified in Table 3, based on the four sets of the parameter values in the normal form (15). Then we use the results presented in Table 3 with a nonlinear analysis based on normal form theory to classify the Hopf bifurcations appearing in Table 2, and the results are shown in Table 4.

To illustrate the analytical results given in Tables 2 and 4, we provide the bifurcation diagrams in Figures 4 (1)-(8). These figures depict the uninfected equilibrium \bar{E}_0 and the infected equilibrium \bar{E}_1 in blue and red, respectively. The solid and dashed lines differentiate stable and unstable states of the equilibrium solutions. The bifurcation points on the equilibrium solutions are highlighted by solid black dots. Moreover, ‘Transcritical’, ‘Turning’,

‘Hopf_{sub}’, and ‘Hopf_{super}’, are used to denote *Transcritical bifurcation*, *Turning point*, *subcritical Hopf bifurcation*, and *supercritical Hopf bifurcation*, respectively. Simulated time histories are used to validate the analytical results, and to show different dynamical behaviors in each case listed in Tables 2 and 4. Subcritical Hopf bifurcation occurs in Cases 1-3, shown in Figures 4 (1)-(3). $A = 0.8$ is used in Figure 4 (1) for Case 1. Choosing $B = 0.036$, we have $E_0 = [17.1282566, 0.023689]$ and $E_1 = [2.233533, 0.8726886]$. The simulated solution converges to E_0 or E_1 , with initial condition taken as $IC_d = [17.13, 0.024]$ or $IC_c = [2.233, 0.873]$, shown in Figures 4 (1d) and (1c), respectively. Figures 4 (1a) and (1b), on the other hand, show the unstable limit cycle bifurcating from the subcritical Hopf bifurcation with $IC_c = [2.233, 0.873]$.

Figure 4 (2) corresponds to Case 2 with $A = 0.71$. Choosing $B = 0.0572 \in [B_S, B_H]$ yields recurrence, independent of the initial conditions, see, for example, the result given in Figure 4 (2b) with $IC_b = [2.4, 0.5]$. However, for $B = 0.06 > B_H$, the simulated time history converges to E_1 , with an initial condition close to E_1 , such as $IC_a = [2.4, 0.6]$ as shown in Figure 4 (2a); or shows recurrence with an initial condition far away from E_1 , such as $IC_c = [2.4, 0.4]$, as shown in Figure 4 (2c).

Figure 4 (3) plots the result for Case 3 with $A = 0.6$, and shows a broader region between the transcritical and Hopf bifurcation points, associated with a larger recurrent region. Recurrence occurs independent of the initial conditions for $B = 0.083 \in [B_S, B_H]$, giving $E_0 = [12.048, 0]$ and $E_1 = [2.576, 0.852]$, as shown in Figures 4 (3a) and (3b), with $IC_a = [2.7, 0.84]$ and $IC_b = [14, 0.1]$, respectively. But if we choose $B = 0.07 > B_H$, we have $E_0 = [14.286, 0]$ and $E_1 = [2.67, 0.8478]$. The time history converges to E_1 with $IC_c = [2.6, 0.8]$, or shows recurrence with $IC_d = [2.6, 0.1]$, as shown in Figure 4 (3c) and (3d), respectively.

Supercritical Hopf bifurcations occur in Cases 4-7, as shown in Figures 4 (4)-(7). Figure 4 (4) depicts the result for Case 4 with $A = 0.07$. Only one supercritical Hopf bifurcation happens in this case, and gives a large recurrent parameter region between the transcritical and Hopf bifurcation points. Although the simulated recurrent behavior does not depend on initial conditions, the recurrent pattern will fade out with the growth of the value of B from the transcritical point to the Hopf bifurcation point, see Figures 4 (4a) and (4b) with the same $IC_{a,b} = [8, 0.1]$, but different values of B : $B = 0.06$ and $B = 0.09$, respectively.

Figure 4 (5) shows the result for Case 5 with $A = 0.06$. A transcritical bifurcation happens between two supercritical Hopf bifurcations. The recurrent region still starts from the transcritical point and independent of the initial conditions, but is narrower than that shown in Figure 4 (4). The simulated recurrent behavior for this case is conducted at $IC = [12, 0.1]$ and $B = 0.06$. Figure 4 (6) corresponds to Case 6 with $A = 0.05$, and two supercritical Hopf bifurcations occur on the right side of the transcritical bifurcation point, which makes the recurrent region even narrower and the recurrent pattern less obvious, as shown in the simulated time history with $IC = [10, 0.1]$ and $B = 0.06$. Negative backward bifurcations occur in Cases 7 and 8, as shown in Figure 4 (7) and (8). Although two Hopf bifurcations are still present in Case 7, see Figure 4 (7), only a regular oscillating pattern exists. For Case 8, no Hopf bifurcation happens in the biologically feasible part of E_1 , and therefore no more interesting dynamics occur.

In general, backward bifurcation, which occurs above the horizontal axis, is much more likely to induce Hopf bifurcation. A Hopf bifurcation can only occur along the upper branch

of \bar{E}_1 , since \bar{E}_0 only changes its stability at a transcritical bifurcation point, and any point on the lower branch of \bar{E}_1 is a saddle node (Yu et al., submitted for publication). Moreover, Hopf bifurcation can lead to a change in the stability of the upper branch of the infected equilibrium \bar{E}_1 . Thus the system further develops bistable, recurrent, or regular oscillating behavior, corresponding to Cases 1 – 7 in Tables 2 and 4, and in Figures 4 (1)-(7). In particular, bistability happens when both equilibria \bar{E}_0 and \bar{E}_1 share a stable parameter region, see Case 1 in Table 2 and Figure 4 (1).

As for recurrent behavior, we observe that recurrence is more likely to happen if the following two conditions are satisfied for the upper branch of \bar{E}_1 : (1) the equilibrium remains unstable as the bifurcation parameter increases and crosses the transcritical point, where \bar{E}_0 and \bar{E}_1 intersect, such that the two equilibria share an unstable parameter range; and (2) at least one Hopf bifurcation occurs from \bar{E}_1 . As shown in Cases 2-6 in Table 2, and the corresponding Figures 4 (2)-(5), the common recurrent parameter region for both subcritical and supercritical Hopf bifurcations starts beside the transcritical point, and is located entirely in the unstable parameter region of \bar{E}_0 and \bar{E}_1 . The simulated recurrent pattern becomes more pronounced if the value of the bifurcation parameter is close to the transcritical point, but approaches an oscillatory pattern as the parameter diverges from the transcritical point, as shown in Figure 4 (4a) and (4b). In this common recurrent parameter region, recurrence occurs independent of initial conditions; see Figures 4 (3a) and (3b). In addition to the common recurrent region, for subcritical bifurcation, seen in Table 2 for Cases (2) and (3) and Figures 4 (2) and (3), recurrence may also appear on the stable side of the subcritical Hopf bifurcation point with an initial condition close to \bar{E}_1 . Moreover, the subcritical Hopf bifurcation and the transcritical point should be close to each other for a clear recurrent pattern. When this is not the case, the periodic solutions show a more regular oscillating pattern, as compared in Figures 4 (2c) and (3d). Although two Hopf bifurcation points occur in Table 2 for Case 5, see Figure 4 (5), the transcritical point is located inside the unstable range of the upper branch of \bar{E}_1 , between the two Hopf bifurcation points. A recurrent pattern still characterizes the dynamical behavior in this case. However, if the unstable range of \bar{E}_1 , between the two Hopf bifurcation points, is located entirely in the unstable range of \bar{E}_0 , and moves further away from the transcritical point, the recurrent motion gradually becomes a regular oscillation, as shown in Figures 4 (6) and (7).

Summarizing the results and discussions presented in the previous two sections, we have the following observations.

1. Due to the fact that \bar{E}_0 only changes its stability at the transcritical bifurcation point, and the fact that any point on the lower branch of \bar{E}_1 is a saddle node, Hopf bifurcation can only occur from the upper branch of \bar{E}_1 . A Hopf bifurcation may result in convergent, recurrent, bistable, or regular oscillating behaviors.
2. Backward bifurcation gives rise to two branches in the infected equilibrium \bar{E}_1 . Hopf bifurcation is more likely to happen when the turning point of the backward bifurcation is located on the positive part of the equilibrium solution in the bifurcation diagram, as shown in Figures 4 (2)-(6). This means that we have two biologically feasible infected equilibria, which is essential to observe bistability, as shown in Figure 4 (1).
3. However, if the turning point on the infected equilibrium \bar{E}_1 , or the backward bifurcation

moves down to the negative part of a state variable in the bifurcation diagram, that is, negative backward bifurcation occurs, then Hopf bifurcation is very unlikely to happen. Although Figure 4 (7) shows an exceptional case, the parameter range for such a Hopf bifurcation is very narrow.

4. The bifurcation diagram for system (4) with $A = 0.03$, shown in Figure 4 (8), is a typical model with negative backward bifurcation. Such negative backward bifurcation may occur in higher-dimensional systems. However, by considering more state variables, which make the system more complicated, Hopf bifurcation can happen in the upper branch of the negative backward bifurcation. We will discuss this possibility in more detail in the next section by examining an autoimmune disease model.

The results obtained in this section suggest the following summary.

Remark 2 *If a disease model contains a backward bifurcation on an equilibrium solution, then as the system parameters are varied, there may exist none, one or two Hopf bifurcations from the equilibrium solution, which may be supercritical or subcritical. If further this equilibrium has a transcritical bifurcation point at which it exchanges its stability with another equilibrium, then recurrence can occur between the transcritical and Hopf bifurcation points and near the transcritical point, where both equilibrium solutions are unstable, and bistability happens when Hopf bifurcation makes a shared stable parameter region for both equilibria.*

6 Negative backward bifurcation in an autoimmune disease model

In the previous section, we examined three cases of negative backward bifurcation: Table 1 Case 4 for system (7) and Table 2 Case (7) and (8) for system (4). The analytical and numerical results showed that solutions typically converge to the infected equilibrium in these cases, and the parameter range for Hopf bifurcation is very limited. As a result, negative backward bifurcation tends to give no interesting behavior. In this section, however, we shall explore an established autoimmune model [1] in which negative backward bifurcation occurs. We demonstrate that after modification, the autoimmune model can also exhibit recurrence.

The autoimmune model [1] takes the form

$$\begin{aligned}
 \frac{dA}{dt} &= f\tilde{v}G - (\sigma_1 R_n + b_1)A - \mu_A A \\
 \frac{dR_n}{dt} &= (\pi_1 E + \beta)A - \mu_n R_n \\
 \frac{dE}{dt} &= \lambda_E A - \mu_E E \\
 \frac{dG}{dt} &= \gamma E - \tilde{v}G - \mu_G G,
 \end{aligned} \tag{16}$$

where mature pAPCs (A) undergo maturation by intaking self-antigen (G), at rate $f\tilde{v}$, and are suppressed by specific regulatory T cells, T_{Reg} cells (R_n), at rate σ_1 ; b_1 represents additional

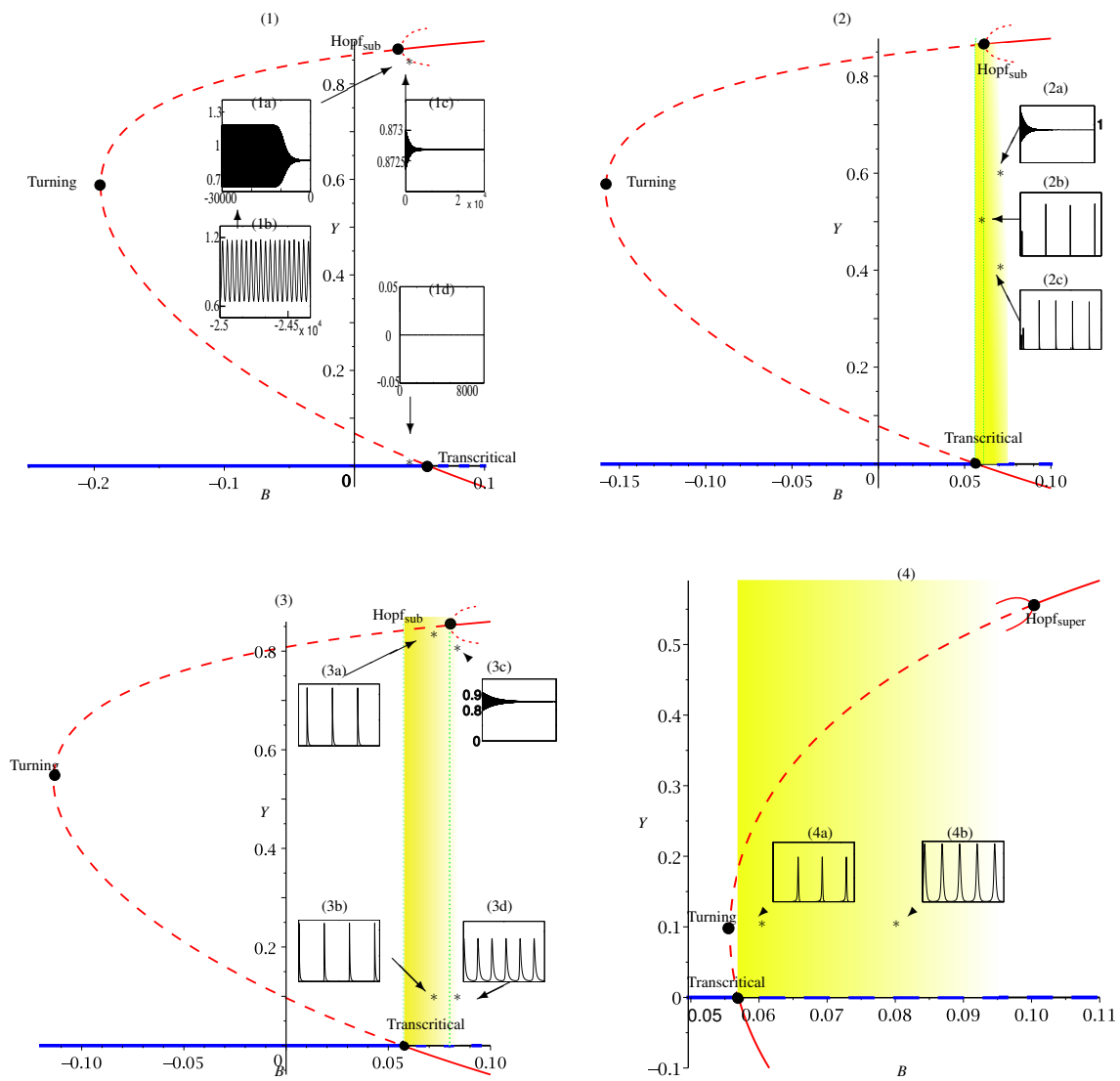


Figure 4: Dynamical behaviors of system (4) corresponding to eight cases listed in Table 2 and 4. All insets are simulated time histories of Y vs. t . The yellow areas fading to white show regions in which recurrent behavior occurs and fades to regular oscillations.

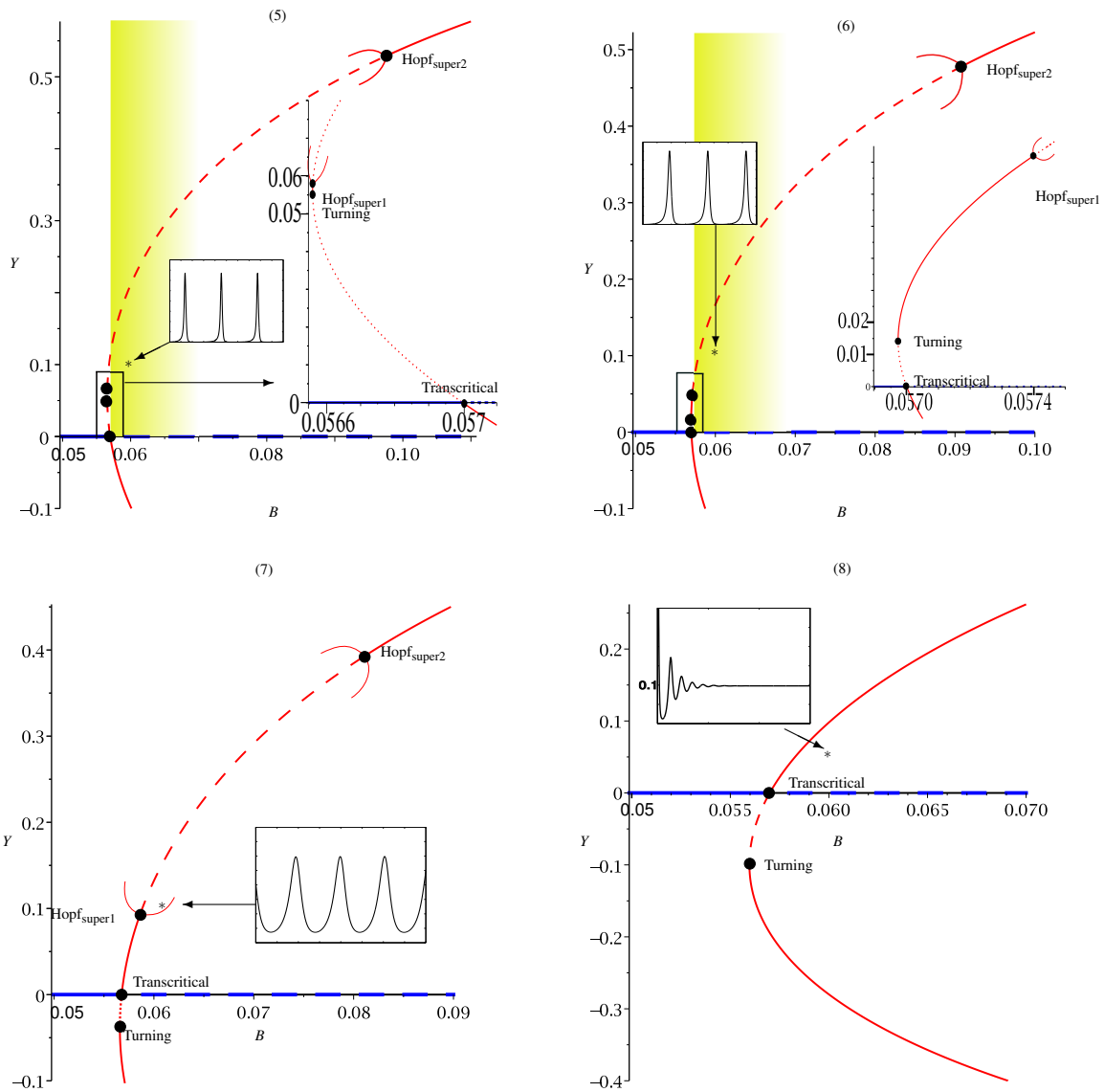


Figure 4: Dynamical behaviors of system (4) corresponding to eight cases listed in Table 2 and 4. All insets are simulated time histories of Y vs. t . The yellow areas fading to white show regions in which recurrent behavior occurs and fades to regular oscillations.

non-specific background suppression. The T_{Reg} cells are activated by mature pAPCs at a rate proportional to the number of auto-reactive effector T cells (E) at rate π_1 , and by other sources at rate β . Active auto-reactive effector T cells (E) come from the activation process initiated by mature pAPCs, at rate λ_E , then attack healthy body tissue and release free self-antigen (G) at rate γ , which is ready for mature pAPCs to engulf; the antigen engulfing rate is $\tilde{\nu}$. The death rates of the populations A , R_n , E , and G are denoted by μ_A , μ_n , μ_E , and μ_G , respectively.

Following the steps described by Zhang et al. (submitted for publication), system (16), can be reduced via quasi-steady state analysis to a 2-dimensional system:

$$\begin{aligned}\frac{dA}{dt} &= \left[\frac{f\tilde{\nu}\gamma\lambda_E}{\mu_E(\tilde{\nu} + \mu_G)} - b_1 - \mu_A \right] A - \sigma_1 R_n A, \\ \frac{dR_n}{dt} &= \left(\frac{\pi_1 \lambda_E}{\mu_E} A + \beta \right) A - \mu_n R_n.\end{aligned}\tag{17}$$

For simplicity, we set $a = \frac{f\tilde{\nu}\gamma\lambda_E}{\mu_E(\tilde{\nu} + \mu_G)} - b_1 - \mu_A$ and $b = \frac{\pi_1 \lambda_E}{\mu_E}$. For the stability and bifurcation analysis, we choose λ_E as the bifurcation parameter. System (17) has a disease-free equilibrium $\bar{E}_0 = (0, 0)$, which is stable if $a > 0$ or $\lambda_E > \frac{(b_1 + \mu_A)(\tilde{\nu} + \mu_G)\mu_E}{f\tilde{\nu}\gamma}$; and unstable if $a < 0$ or $\lambda_E < \frac{(b_1 + \mu_A)(\tilde{\nu} + \mu_G)\mu_E}{f\tilde{\nu}\gamma}$. Thus a static bifurcation occurs on \bar{E}_0 when $a = 0$ or $\lambda_E = \frac{(b_1 + \mu_A)(\tilde{\nu} + \mu_G)\mu_E}{f\tilde{\nu}\gamma}$. The disease equilibrium is given by $\bar{E}_1 = (\bar{A}, \bar{R}_n)$, in which $\bar{R}_n = \frac{(b\bar{A} + \beta)\bar{A}}{\mu_n}$, and \bar{A} is given by the roots of the following equation,

$$f_8(A) = b\sigma_1 A^2 + \beta\sigma_1 A - \mu_n a.\tag{18}$$

Equation (18) has two roots with negative signs if $a < 0$, with opposite signs if $a > 0$, and only one zero root if $a = 0$. This means that a negative backward bifurcation is possible in system (17) with proper parameter values. We further examine the characteristic equation at \bar{E}_1 , which shares the same form as equation (13), with $\text{Tr}(J|_{\bar{E}_1}) = \frac{1}{\mu_n}(b\sigma_1 A^2 + \beta\sigma_1 A + \mu_n^2 - a\mu_n) := a_{11}$ and $\text{Det}(J|_{\bar{E}_1}) = 3b\sigma_1 A^2 + 2\beta\sigma_1 A - a\mu_n := a_{12}$. Solving $f_8(A) = 0$ and $a_{12} = \text{Det}(J|_{\bar{E}_1}) = 0$, gives the static bifurcation point of \bar{E}_1 at $(\bar{A}, a) = (0, 0)$ or $(\bar{A}, \lambda_E) = (0, \frac{(b_1 + \mu_A)(\tilde{\nu} + \mu_G)\mu_E}{f\tilde{\nu}\gamma})$, which is a transcritical bifurcation point between \bar{E}_0 and \bar{E}_1 . Moreover, Hopf bifurcation can happen if and only if $f_8(A) = 0$ and $a_{11} = \text{Tr}(J|_{\bar{E}_1}) = 0$, which can be satisfied only if $\mu_n = 0$. This implies that the positive branch of \bar{E}_1 is stable for any positive values of μ_n . Thus, this model cannot exhibit recurrence, bistability, or even regular oscillation. The same conclusion was obtained in Zhang et al., (submitted for publication) for the original 4-dimensional model (16).

However, a recent experimental discovery [3] has revealed a new class of terminally differentiated T_{Reg} cells. As described in detail in Zhang et al., (submitted for publication), introducing this cell population, denoted R_d , into the model yields the full system

$$\begin{aligned}\frac{dA}{dt} &= f\tilde{\nu}G - \sigma_1(R_n + dR_d)A - (b_1 + \mu_A)A \\ \frac{dR_n}{dt} &= (\pi_1 E + \beta)A - \mu_n R_n - \xi R_n \\ \frac{dR_d}{dt} &= c\xi R_n - \mu_d R_d \\ \frac{dE}{dt} &= \lambda_E A - \mu_E E \\ \frac{dG}{dt} &= \gamma E - \tilde{\nu}G - \mu_G G\end{aligned}$$

and quasi-steady state analysis then yields a reduced 3-dimensional model in the form

$$\begin{aligned}\frac{dA}{dt} &= \left[\frac{f\tilde{v}\gamma\lambda_E}{(\tilde{v}+\mu_G)\mu_E} - (b_1 + \mu_A) \right] A - \sigma_1(R_n + dR_d)A, \\ \frac{dR_n}{dt} &= \left(\frac{\pi_1\lambda_E}{\mu_E} A + \beta \right) A - \mu_n R_n - \xi R_n, \\ \frac{dR_d}{dt} &= c\xi R_n - \mu_d R_d.\end{aligned}$$

Again, here λ_E is chosen as the bifurcation parameter for stability and bifurcation analysis. It is easy to show that system (6) still has a disease-free equilibrium \bar{E}_0 as $(A, R_n, R_d) = (0, 0, 0)$, and a disease equilibrium \bar{E}_1 as $(\bar{A}, \bar{R}_n, \bar{R}_d)$, where $\bar{R}_d = \frac{c\xi\bar{R}_n}{\mu_d}$, $\bar{R}_n = \frac{\beta\mu_E + \pi_1\lambda_E\bar{A}}{\mu_E(\mu_n + \xi)}\bar{A}$, and \bar{A} is determined from the following quadratic equation:

$$f_9(A) = \pi_1\lambda_E A^2 + \beta\mu_E A + \frac{\mu_d(\mu_n + \xi)}{(\tilde{v} + \mu_G)(cd\xi + \mu_d)\sigma_1} [-f\gamma\tilde{v}\lambda_E + (b_1 + \mu_A)(\mu_G + \tilde{v})\mu_E],$$

which gives two negative roots if $\lambda_E < \lambda_{ES} = \frac{(b_1 + \mu_A)(\mu_G + \tilde{v})\mu_E}{f\gamma\tilde{v}}$, and two roots with opposite signs when $\lambda_E > \lambda_{ES}$. The critical point is determined by $\lambda_E = \lambda_{ES}$, which is actually the intersection point of \bar{E}_0 and \bar{E}_1 . The two equilibrium solutions exchange their stability at λ_{ES} , leading to a transcritical bifurcation at $(\bar{A}, \lambda_E) = (0, \lambda_{ES})$. Note that the negative backward bifurcation still happens in system 6. Moreover, a Hopf bifurcation occurs from the upper branch of \bar{E}_1 , giving rise to oscillation and recurrence.

Realistic parameter values have been obtained in Zhang et al., (submitted for publication), and are given as follows:

$$\begin{aligned}f &= 1 \times 10^{-4}, \quad \tilde{v} = 0.25 \times 10^{-2}, \quad \sigma_1 = 3 \times 10^{-6}, \quad b_1 = 0.25, \quad \mu_A = 0.2, \quad \pi_1 = 0.016, \\ \beta &= 200, \quad \mu_n = 0.1, \quad \mu_E = 0.2, \quad \gamma = 2000, \quad \mu_G = 5, \quad \mu_d = 0.2, \quad c = 8, \quad d = 2, \quad \xi = 0.025.\end{aligned}$$

For the above parameter values, the Hopf critical point is obtained at $(A_H, \lambda_{EH}) = (5.6739, 1691.6414)$, while the turning point is at $(A_T, \lambda_{ET}) = (-1.4205, 879.9848)$, and the transcritical bifurcation point is at $(A_S, \lambda_{ES}) = (0, 900.45)$. These three bifurcation points and the stability of equilibrium solutions are shown in the bifurcation diagram given in Figure 5(a), and the simulated recurrent time history is plotted in Figure 5(b) for $\lambda_E = \lambda_{EH} + 1000$.

In summary, when negative backward bifurcation occurs, that is, the turning point is located in the negative state variable space, less complex dynamical behavior will be present. Hopf bifurcation in a biologically feasible area does not happen in the reduced 2-dimensional system (17), nor in the original system (16) (Zhang et al., submitted for publication). However, if we increase the dimension of the system, Hopf bifurcation and complex dynamical phenomena can emerge, as shown in our results for system (6).

7 Conclusion

In this paper, we first review previous work on a reduced 2-dimensional infection model with a concave incidence rate [28]. The authors proved that the disease equilibrium will emerge and be globally stable when the basic reproduction number R_0 is greater than 1. This means that no complex dynamical phenomenon can occur in such models. However, by adding an

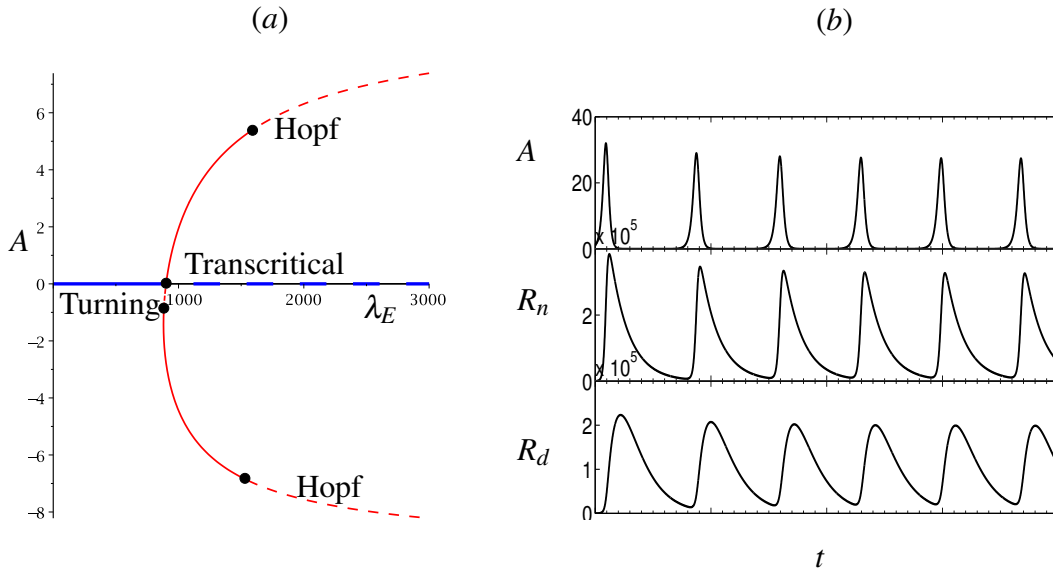


Figure 5: Dynamics of system (17): (a) bifurcation diagram; and (b) simulated time history for $\lambda_E = \lambda_{EH} + 1000$.

extra saturating treatment term to this simple 2-dimensional infection model, the resulting system (6) considered in [49] can exhibit backward bifurcation, which increases the parameter range for Hopf bifurcation, which in turn leads to recurrent, bistable and regular oscillating behaviors.

Instead of adding an extra term, a 2-dimensional infection model with a convex incidence function can likewise show rich dynamics due to the occurrence of backward bifurcation, giving rise to two types of Hopf bifurcation. Biologically, a convex incidence rate implies that existing infection makes the host more vulnerable to further infection, showing a cooperative effect in disease progression. From the view point of mathematics, the convex incidence function enables backward bifurcation to occur on the positive branch of the disease equilibrium solution, which further generates Hopf bifurcation. The location and direction of Hopf bifurcation(s), determined by parameter values, can further give rise to bistable, recurrent, and regular oscillating behaviors.

Cooperative effects also occur during the progression of autoimmune disease. However, for an autoimmune model with negative backward bifurcation, in which the turning point is located on the negative state variable space, the biologically feasible parameter range in which Hopf bifurcation may occur is limited. By introducing an additional state variable to the autoimmune model, recurrent phenomenon are once again observed.

References

- [1] H. K. Alexander and L. M. Wahl. Self-tolerance and autoimmunity in a regulatory T cell model. *Bulletin of mathematical biology*, 73(1):33–71, 2011.
- [2] J. Arino, C. C. McCluskey, and P. van den Driessche. Global results for an epidemic

- model with vaccination that exhibits backward bifurcation. *SIAM Journal on Applied Mathematics*, 64(1):260–276, 2003.
- [3] C. Baecher-Allan, E. Wolf, and D. A. Hafler. MHC class II expression identifies functionally distinct human regulatory T cells. *The Journal of Immunology*, 176:4622–4631, 2006.
- [4] K. W. Blayneh, A. B. Gumel, S. Lenhart, and T. Clayton. Backward bifurcation and optimal control in transmission dynamics of west nile virus. *Bulletin of Mathematical Biology*, 72(4):1006–1028, 2010.
- [5] F. Brauer. Backward bifurcations in simple vaccination models. *Journal of Mathematical Analysis and Applications*, 298(2):418 – 431, 2004.
- [6] C. J. Briggs and H. C. J. Godfray. The dynamics of insect-pathogen interactions in stage-structured populations. *American Naturalist*, pages 855–887, 1995.
- [7] G. C. Brown and R. Hasibuan. Conidial discharge and transmission efficiency of *neozygites floridana*, an entomopathogenic fungus infecting two-spotted spider mites under laboratory conditions. *Journal of Invertebrate Pathology*, 65(1):10 – 16, 1995.
- [8] V. Capasso and G. Serio. A generalization of the kermack-mckendrick deterministic epidemic model. *Mathematical Biosciences*, 42(1):43–61, 1978.
- [9] C. Castillo-Chavez, K. Cooke, W. Huang, and S. Levin. On the role of long incubation periods in the dynamics of acquired immunodeficiency syndrome (aids). part 2: Multiple group models. In Carlos Castillo-Chavez, editor, *Mathematical and Statistical Approaches to AIDS Epidemiology*, volume 83 of *Lecture Notes in Biomathematics*, pages 200–217. Springer Berlin Heidelberg, 1989.
- [10] C. Castillo-Chavez, Cooke K., Huang W., and Levin S. A. Results on the dynamics for models for the sexual transmission of the human immunodeficiency virus. *Applied Mathematics Letters*, 2(4):327 – 331, 1989.
- [11] A. C. Collier, R. W. Coombs, D. A. Schoenfeld, R. L. Bassett, J. Timpone, A. Baruch, M. Jones, K. Facey, C. Whitacre, V. J. McAuliffe, H. M. Friedman, T. C. Merigan, R. C. Reichman, C. Hooper, and L. Corey. Treatment of human immunodeficiency virus infection with saquinavir, zidovudine, and zalcitabine. *New England Journal of Medicine*, 334(16):1011–1018, 1996.
- [12] J. M. Conway and D. Coombs. A stochastic model of latently infected cell reactivation and viral blip generation in treated HIV patients. *PLoS Computational Biology*, 7(4), 2011.
- [13] W. R. Derrick and P. Driessche. A disease transmission model in a nonconstant population. *Journal of Mathematical Biology*, 31(5):495–512, 1993.

- [14] G. Dornadula, H. Zhang, B. VanUitert, J. Stern, L. Livornese Jr., M. J. Ingerman, J. Witek, R. J. Kedanis, J. Natkin, J. DeSimone, and R. J. Pomerantz. Residual HIV-1 RNA in blood plasma of patients taking suppressive highly active antiretroviral therapy. *Journal of the American Medical Association*, 282(17):1627–1632, 1999.
- [15] J. Dushoff, W. Huang, and C. Castillo-Chavez. Backwards bifurcations and catastrophe in simple models of fatal diseases. *Journal of mathematical biology*, 36(3):227–248, 1998.
- [16] C. Fraser, N. M. Ferguson, F. de Wolf, and R. M. Anderson. The role of antigenic stimulation and cytotoxic T cell activity in regulating the long-term immunopathogenesis of HIV: mechanisms and clinical implications. *Proceedings of the Royal Society B: Biological Sciences*, 268(1481):2085–2095, 2001.
- [17] I. C. H. Fung, M. Gambhir, A. van Sighem, F. de Wolf, and G. P. Garnett. The clinical interpretation of viral blips in HIV patients receiving antiviral treatment: Are we ready to infer poor adherence? *Journal of Acquired Immune Deficiency Syndromes*, 60(1):5–11, 2012.
- [18] N. J. Garretta, V. Apeaa, A. Noria, I. Ushiro-Lumbb, A. R. Oliverb, G. Bailya, and D. A. Clarkb. Comparison of the rate and size of HIV-1 viral load blips with Roche COBAS TaqMan HIV-1 versions 1.0 and 2.0 and implications for patient management. *Journal of Clinical Virology*, 53(4):354–355, 2012.
- [19] L. Gil and et al. Contribution to characterization of oxidative stress in hiv/aids patients. *Pharmacological research*, 47(3):217–224, 2003.
- [20] J. T. Grennan, M. R. Loutfy, D. Su, P. R. Harrigan, C. Cooper, M. Klein, N. Machouf, J. S. G. Montaner, S. Rourke, C. Tsoukas, B. Hogg, J. Raboud, and the CANOC Collaboration. Magnitude of virologic blips is associated with a higher risk for virologic rebound in HIV-infected individuals: A recurrent events analysis. *Journal of Infectious Diseases*, 205(8):1230–1238, 2012.
- [21] H. Gmez-Acevedo and M. Y. Li. Backward bifurcation in a model for htlv-i infection of cd4+ t cells. *Bulletin of Mathematical Biology*, 67(1):101 – 114, 2005.
- [22] K. P. Hadeler and P. Van den Driessche. Backward bifurcation in epidemic control. *Mathematical Biosciences*, 146(1):15–35, 1997.
- [23] H. W. Hethcote, M. A. Lewis, and P. Van Den Driessche. An epidemiological model with a delay and a nonlinear incidence rate. *Journal of mathematical biology*, 27(1):49–64, 1989.
- [24] H. W. Hethcote and P. Van den Driessche. Some epidemiological models with nonlinear incidence. *Journal of Mathematical Biology*, 29(3):271–287, 1991.
- [25] W. Huang, K. L. Cooke, and C. Castillo-Chavez. Stability and bifurcation for a multiple-group model for the dynamics of hiv/aids transmission. *SIAM Journal on Applied Mathematics*, 52(3):835–854, 1992.

- [26] N. Israel and M. A. Gougerot-Pocidalò. Oxidative stress in human immunodeficiency virus infection. *Cell Molec Life Sciences*, 53(11-12):864–870, 1997.
- [27] L. E. Jones and A. S. Perelson. Opportunistic infection as a cause of transient viremia in chronically infected HIV patients under treatment with HAART. *Bulletin of Mathematical Biology*, 67(6):1227–1251, 2005.
- [28] A. Korobeinikov and P. K. Maini. Non-linear incidence and stability of infectious disease models. *Mathematical Medicine and Biology*, 22(2):113–128, 2005.
- [29] M. Y. Li and J. S. Muldowney. Global stability for the seir model in epidemiology. *Mathematical Biosciences*, 125(2):155–164, 1995.
- [30] N. Li and M. Karin. Is $\text{nf-}\kappa\text{b}$ the sensor ooxoxidative stress? *The FASEB Journal*, 13(10):1137–1143, 1999.
- [31] W. Liu, H. W. Hethcote, and S. A. Levin. Dynamical behavior of epidemiological models with nonlinear incidence rates. *Journal of Mathematical Biology*, 25(4):359–380, 1987.
- [32] W. Liu, S. Levin, and Y. Iwasa. Influence of nonlinear incidence rates upon the behavior of sirs epidemiological models. *Journal of Mathematical Biology*, 23(2):187–204, 1986.
- [33] J. D. Murray. *Mathematical Biology: I. An Introduction*. Interdisciplinary Applied Mathematics. Springer, 2002.
- [34] S. Palmer, F. Maldarelli, A. Wiegand, B. Bernstein, G. J. Hanna, S. C. Brun, D. J. Kempf, J. W. Mellors, J. M. Coffin, and M. S. King. Low-level viremia persists for at least 7 years in patients on suppressive antiretroviral therapy. *Proceedings of the National Academy of Sciences*, 105(10):3879–3884, 2008.
- [35] S. Palmer, A. P. Wiegand, F. Maldarelli, H. Bazmi, J. M. Mican, M. Polis, R. L. Dewar, A. Planta, S. Liu, J. A. Metcalf, J. W. Mellors, and J. M. Coffin. New real-time reverse transcriptase-initiated PCR assay with single-copy sensitivity for human immunodeficiency virus type 1 RNA in plasma. *Journal of Clinical Microbiology*, 41(10):4531–4536, 2003.
- [36] L. Rong and A. S. Perelson. Asymmetric division of activated latently infected cells may explain the decay kinetics of the HIV-1 latent reservoir and intermittent viral blips. *Mathematical Biosciences*, 217(1):77–87, 2009.
- [37] L. Rong and A. S. Perelson. Modeling latently infected cell activation: viral and latent reservoir persistence, and viral blips in HIV-infected patients on potent therapy. *PLoS Computational Biology*, 5(10):e1000533, 2009.
- [38] S. Ruan and W. Wang. Dynamical behavior of an epidemic model with a nonlinear incidence rate. *Journal of Differential Equations*, 188(1):135 – 163, 2003.
- [39] K. B. Schwarz. Oxidative stress during viral infection: a review. *Free Radical Biology and Medicine*, 21(5):641–649, 1996.

- [40] C. P. Simon and J. A. Jacquez. Reproduction numbers and the stability of equilibria of si models for heterogeneous populations. *SIAM journal on Applied Mathematics*, 52(2):541–576, 1992.
- [41] C. B. Stephenson, G. S. Marquis, S. D. Douglas, and C. M. Wilson. Immune activation and oxidative damage in HIV-positive and HIV negative adolescents. *Journal of Acquired Immune Deficiency Syndromes*, 38(2):180–190, 2005.
- [42] P. van den Driessche and J. Watmough. Reproduction numbers and sub-threshold endemic equilibria for compartmental models of disease transmission. *Mathematical Biosciences*, 180(12):29 – 48, 2002.
- [43] R. D. van Gaalen and L. M. Wahl. Reconciling conflicting clinical studies of antioxidant supplementation as HIV therapy: a mathematical approach. *BMC Public Health*, 9(Suppl. 1):1–18, 2009.
- [44] S. Wiggins. *Introduction to Applied Nonlinear Dynamical Systems and Chaos*. Berlin etc., Springer-Verlag, 1990.
- [45] W. Yao, L. Hertel, and L. M. Wahl. Dynamics of recurrent viral infection. *Proceedings of the Royal Society - Biological Sciences*, 273(1598):2193–2199, 2006.
- [46] P. Yu. Computation of normal forms via a perturbation technique. *Journal of Sound and Vibration*, 211(1):19–38, 1998.
- [47] W. Zhang, L. Wahl, and P. Yu. Conditions for transient viremia in deterministic in-host models: Viral blips need no exogenous trigger. *SIAM Journal on Applied Mathematics*, 73(2):853–881, 2013.
- [48] W. Zhang, L. Wahl, and P. Yu. Viral blips may not need a trigger: How transient viremia can arise in deterministic in-host models. *SIAM Review*, 56(1):127–155, 2014.
- [49] L. Zhou and M. Fan. Dynamics of an SIR epidemic model with limited medical resources revisited. *Nonlinear Analysis: Real World Applications*, 13(1):312 – 324, 2012.